Rev. Adv. Mater. Sci. 35 (2013) 59-66

# INFLUENCE OF THE CARBON-BASED SUPPORT ON THE ELECTROCHEMICAL BEHAVIOR OF NANOCOMPOSITES WITH Cu-Sn NANOPARTICLES

**I.N. Markova[1], Olivier Chauvet[2], T.I. Petrov[1], V.P. Stefanova[1], I.D. Denev[1] and S.A. Uzunova[1]**

[1]University of Chemical Technology and Metallurgy, 8, Kliment Ohridski blvd., 1756 Sofia, Bulgaria
[2] Institute of materials, 2, rue de la Houssinière B.P.32229, 44322 Nantes cedex 3 – France

*Received : October 22, 2013*

**Abstract.** Cu-Sn nanoparticle powder have been synthesized through a borohydride reduction in a mixture of water solutions of chloride salts and also applying a template technique using a support. As supports for the template synthesis of the Cu-Sn nanoparticle have been used carbon foam (C-foam), carbon powder (C-powder) and graphite. It has been examined the influence of the support on the formation and phase composition of the obtained nanoparticles. X-ray diffraction (XRD), scanning electron microscopy (SEM), and electrochemical analyses of the carbon-based (C-based) nanocomposites with Cu-Sn nanoparticles have been carried out. $Cu_6Sn_5$ and $Cu_{10}Sn_3$ phases are formed depending on the support used. The obtained C-based nanocomposites exhibit a different electrochemical behavior depending on the C-based support and respectively the particle size and their phase composition. According to the carbon matrix different nanocomposites are formed such as graphite/$Cu_{10}Sn_3$, $Cu_6Sn_5$, $Cu_2O$; C-powder/$Cu_6Sn_5$, $Cu_2O$; C-foam/ $Cu_{10}Sn_3$,Cu,Sn. The composite of graphite/Cu-Sn alloy is characterized by the highest irreversible discharge capacity of 62%, lower efficiency of the first cycle of 38% and the highest average discharge capacity of 410 mAh $g^{-1}$, while the composite of C-foam/Cu-Sn alloy is characterized by the highest efficiency at the first cycle of 73%.

## 1. INTRODUCTION

The high energy Li-ion cells are needed anode materials with a significantly higher specific capacity than that of the graphite. This demands the development of new technologies to optimize the existing and conventionally used carbonaceous materials [1-3].

The major problem when carbonaceous materials are used refers to the high irreversible capacity during the first cycle, due to the irreversible absorption of lithium in the electrode structure and the formation of a protective solid electrolyte interface (SEI) film onto the electrode surface [4-6]. This problem requires the additional amount of lithium in the cell. It can be supplied from the positive electrode, which leads to the necessity of an extra amount of active material.

Another problem of the carbon electrodes is their relatively low gravimetric capacity (372 Ah $kg^{-1}$), as well as the final potential of the lithium insertion, which is similar to that of its precipitation.

Recently, some binary or ternary lithium alloys, intermetallic alloys and tin oxide glasses have attracted worldwide attention. In particular, tin was used as an active element, because it can combine with Li to form $Li_{22}Sn_5$ alloys with a theoretical capacity of 990 Ah $kg^{-1}$ [7-10]. But the major disadvantage of the tin and tin alloys is volumetric

Corresponding author: I.N. Markova, e-mail : vania@uctm.edu

expansion during lithium intercalation, which leads to a microstructuring, loss of contact between the particles and deterioration of the electrode mechanical stability [11,12].

The main strategies to overcome the problems of the anodes based on alloys are associated with the control of the active material morphology and preparation of multiphase composites. The reduction of the particle size of the active material in most cases leads to a smaller volume changes during a cycling. Regardless of the relative volumes for the nanosized and large granular materials are retained, their absolute volume changes are different. The preparation of multiphase composites is related with an improvement of the material cycliability. Usually the various single phases reacte one after another at different potentials and the non-reacting phases can buffer the volume changes of the reacting phase [13,14].

During the last years the efforts of many researchers and manufacturers have been aimed to obtain carbon-based metal composite materials, which can actually solve the problems of the conventional anodes (graphites or alloys), combining the unique properties of the both components. In this way it is realized a high energy matrix with stable electrochemical parameters [15,16].

When carbon-tin composites are used, the carbon acts as a matrix for a lithium storage and also at the same time prevents the volumetric expansion of the metal. In this case the high capacity due to the lithium storage by the help of tin is combined with the stability and elasticity of carbon matrix during a cycling [17-20].

The cycliability of the composite material can be improved by a depositing of an additional copper coating. The copper plays the role of an inactive matrix, which has a mitigating effect on the volume changes [21].

Different carbonaceous materials such as natural and synthetic graphite, hard carbon, pure carbon can be used as C-matrix. The type of C-matrix influences the electrochemical characteristics of the active material by its morphology and specific surface area.

Some authors have observed a linear relation between the irreversible capacity and the specific surface area. With increasing the specific surface area the irreversible capacity also increases [22]. It is important to note that the developed active surface of the carbon has to be less than 10 $m^2 g^{-1}$ in order to ensure a safety performance of the lithium-ion battery [23].

The purpose of this study was to carry out an electrochemical test of C-based nanocomposites with Cu-Sn nanoparticles obtained by a template synthesis through a borohydride reduction and to establish the influence of the carbon matrix type on the electrochemical behavior of these composites. For this purpose three composites representing a matrix of graphite, C-powder and C-foam coated with nanocrystalline Cu-Sn alloy to be prepared and characterized.

## 2. MATERIALS AND METHODS

Cu-Sn nanoparticles have been synthesized through a borohydride reduction process [24] with 0.2 M $NaBH_4$ in a mixture of water solutions of 0.1M $CuCl_2.2H_2O$ and 0.1 M $SnCl_2.2H_2O$ in a presence of a citric acide $(HOOCCH_2)2C(OH)COOH$ as a complexing agent at a ratio 1:1.2:3.2 at room temperature and atmospheric pressure. A synthesis of Cu-Sn nanoparticles have been also carried out applying a template technique using different supports such as graphite, C-powder, and C-foam at the same technological conditions. The carbon-based nanocomposite materials have been obtained applying the nanoparticle template synthesis (in-situ) using carbon based supports (matrix).

As initial carbon-based materials have been used graphite with a flake morphology type SFC44 of Timcal with a specific surface area of 4.6 ±0.2 $m^2g^{-1}$, C-powder of Alfa Aesar characterized by spherical, micro-carbon grains with a low dispersion with a specific surface area (SSA) of about 20 $m^2 g^{-1}$ and C-foam of Alfa Aesar with a specific surface area of 17.4 $m^2 g^{-1}$.

The C-foam is previously modified applying sensibilisation with a mixture of water solution of $SnCl_2$ and HCl acide and activation with a mixture of water solution of $PdCl_2$ and HCl acide in order to create clusters for nucleation and after that the reaction mixture is added.

After the finishing of the reduction process the samples were filtrated, washed with destilated water and ethanol and dryed in a vaccum during 24 hours at 100 °C. In all obtained samples the supports used regarding the intermetallic Cu-Sn alloy is 80%. The specific surface area was assessed by BET nitrogen adsorption measured in a static volumetric device Area Meter, Strolein.

The morphology and phase composition of the obtained Cu-Sn nanoparticles synthesized with C-based support were examined by a scanning electron microscopy (SEM) and X-ray diffracrion (XRD). The SEM images were made with a JEOL

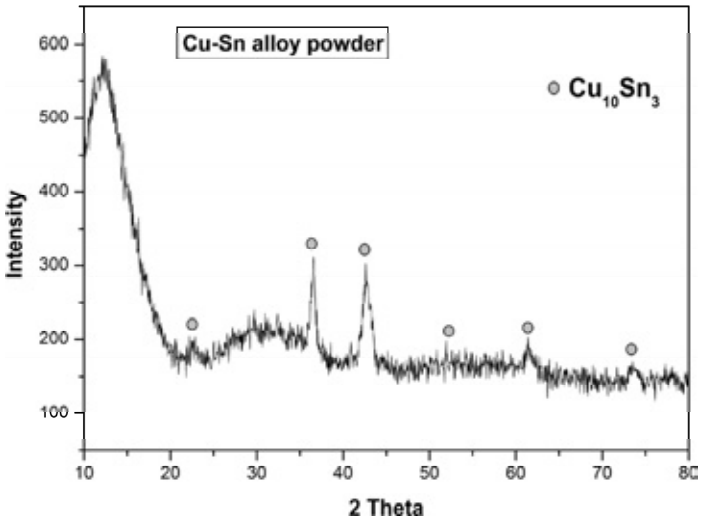


**Fig. 1.** XRD pattern of Cu-Sn nanoparticles obtained by a reductive precipitation method.

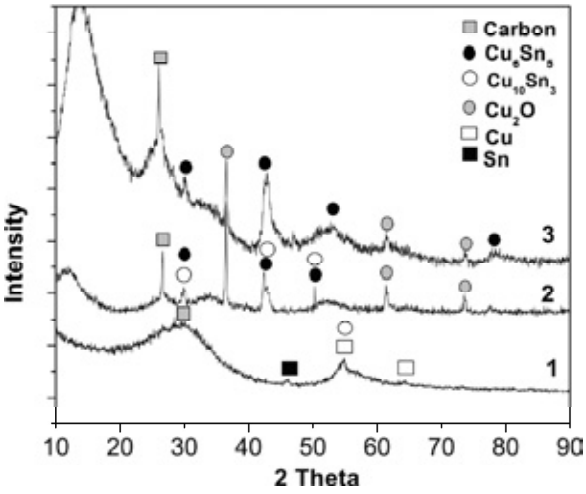


**Fig. 2.** XRD patterns of C-based composites with Cu-Sn nanoparticles obtained using a different support: 1 – C-foam, 2 – graphite, 3 - C-powder.

6400F (Japan) SEM microscope at accelerating voltage of 7 kV. X-ray diffraction patterns of all samples were collected within the 2q range from 10° to 95° with a constant step 0.03° and counting time 1 s/step on Philips PW 1050 diffractometer using $CuK_{\alpha}$ radiation.

The electrochemical behavior of the $Cu_{10}Sn_3$ alloy and the composites (C/Cu-Sn) is investigated in a three-electrode cell using a computer controlled laboratory cycling equipment. The tested nanocomposite electrodes were prepared by mixing of 50% of the active component and 50% of Teflonized Acetylene Black (TAB-2). The mixture was pressed (981 MPa) onto a copper foil substrate with a diameter of 15 mm. Li foil was used as a negative electrode. The electrolyte is a mixture of 1M $LiPF_6$, ethylene carbonate (EC) and diethyl carbonate (DEC) (1:1). The water content in the electrolyte was under 30 ppm. Test cell was assembled in argon-filled glove box. The cell was cycled at room temperature and a constant current density of 0.2 mA $cm^{-2}$ between 0.01 – 1.5 V towards $Li^+/Li$.

## 3. RESULTS AND DISCUSSION

Fig. 1 shows the X-ray diffraction pattern of the Cu-Sn alloy powder synthesized through a borohydride reduction process. The formation of $Cu_{10}Sn_3$ phase is proved.

Fig. 2 presents X-ray diffraction patterns of Cu-Sn nanoparticles deposited using difereent suppotd such as C-foam, C-powder and graphite.

In the case of Cu-Sn nanoparticles synthesized using C-foam as a support a phase of $Cu_{10}Sn_3$ is formed. But phases of Cu and Sn are also observed, as well as the presence of carbon phase is proved.

When C-powder is used as a carrier for the Cu-Sn nanoparticles synthesis the diffraction pattern consists of two phases: major phase of $Cu_6Sn_5$ and the impure phase of $Cu_2O$. The presence of carbon phase is also improved. The presence of impure phase of $Cu_2O$ in the sample indicates that in this systemit has to be expected also the presence of small amount of Sn phase simultaneously, which is not detected by XRD here.

The X-ray diffraction pattern of the nanocomposites based on Cu-Sn nanoparticles and graphite as a support has proven the existence of three phases: the major phases of $Cu_6Sn_5$ and $Cu_{10}Sn_3$ and a little impure phase of $Cu_2O$, as shown in the Fig. 2. A graphite phase is also indicated.

From the peak position and the half-height width of the X-ray diffraction peak, the mean crystallite size is calculated. It is observed that the size of Cu-

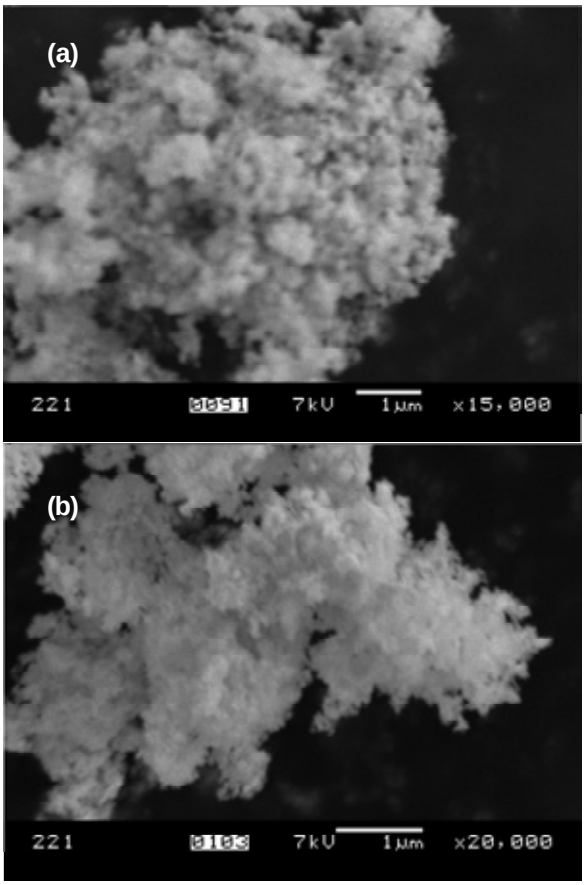


**Fig. 3.** SEM image of Cu-Sn nanoparticles powder prepared by a reductive precipitaion at a different magnification: a-x15000, b-x20000.

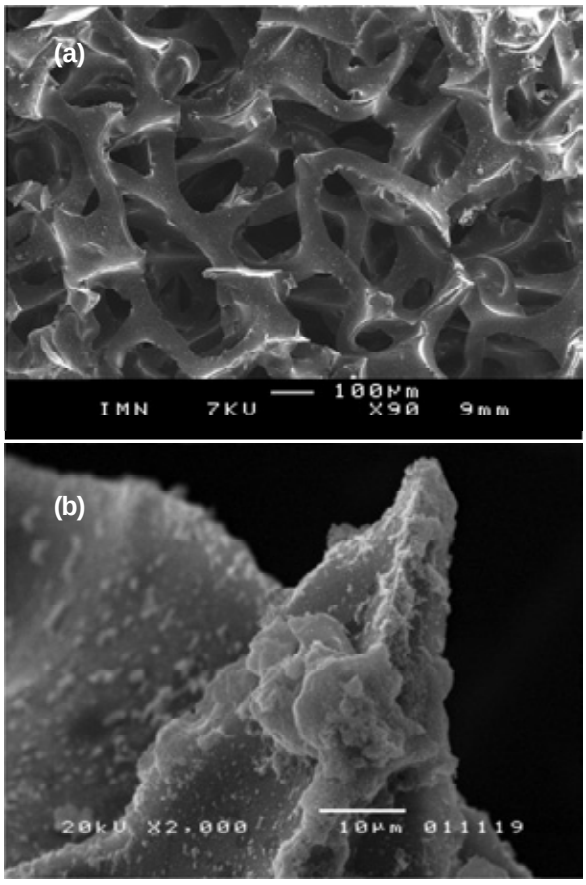


**Fig. 4.** SEM images: a-carbon foam, x90, b-C-foam/ Cu-Sn nanoparticles,x 2000.

Sn particle alloy powder is 40 to 60 nm. The particle size observed from the SEM images is the similar, which is illustrated as follows. Due to aggregation of the nanoparticles together with C-flakes in the case of graphite support microparticles 50-60 mm in size have been formed.

The SEM images of nanosized Cu-Sn powder samples are shown in Figs. 3 - 6. It can be seen that the morphology of four samples have differences. As shown in Fig. 3, the Cu-Sn nanoparticles synthesized through a borohydride reduction in water solutions are too small to be identified and aggregate to large aggregations randomly. It could be contributed to that the strong reducing agent $NaBH_4$ in combination with an intense stiring during the reductive process creates a large number of nuclei, which limited the growth of graines. The small particles with a high surface energy tend to aggregate spontaneously to decreasing their energy.

The SEM images of the support (C-foam) and Cu-Sn nanoparticles deposited using C-foam at a different magnification are shown in Fig. 4. It can be seen that the nanoparticles also exhibite a tendency to aggregate as a result of a high developed surface due to the particle nanosize.

Fig. 5 presents SEM images of C-powder used as a matrix for the nanoparticle template synthesis and respectively of Cu-Sn nanoparticles obtained using the C-powder. Smaller particles and bigger ones are grown on the C-grain surface.

SEM images of a graphite and Cu-Sn nanoparticles synthesized using the graphite support are show in Figs. 6a-6d. Graphite grains irregular and flake in form are observed in Fig. 6a. The SEM image in Fig. 6b shows aggregated Cu-Sn particles obtained together with and between the graphite flakes. Fig. 6c demonstrates microparticles in size of 50-60 μm due to the aggregation of nanoparticles together with the graphite particles. Plates of Sn in size of 5.5x1.5x10 μm are also observed (Fig. 6d).

On the basis of the SEM and XRD results it could be say that the used carbon-based supports (C-foam, C-powder and graphite) influence on the particle size even though weakly and also differently on the phase composition of the formed Cu-Sn nanoparticle alloy powder. The specific surface area (SSA) of

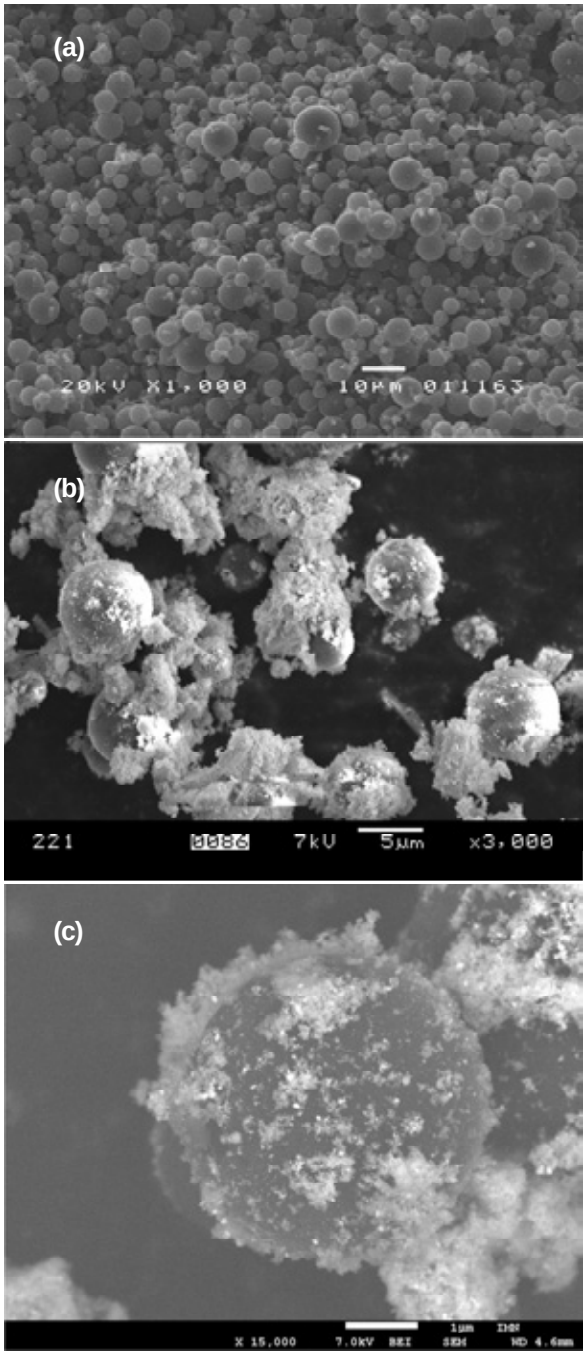


**Fig. 5.** SEM images: a - C-powder, x1000; b, c - C-powder/Cu-Sn nanoparticles at a different magnifications, x3000 and x15000 respectively.

the supports used after the Cu-Sn alloy deposition is changed – in all cases it is decreased.

In the case of Cu-Sn nanoparticles synthesized without using a support the particle size is between 40 to 60 nm and it is observed strongly expressed particle aggregation. Their specific surface area is about 30 $m^2 \cdot g^{-1}$. Phase of $Cu_{10}Sn_3$ is formed.

In the case of Cu-Sn nanoparticles synthesized using C-foam as a support the particle morphology is similar. Aggregated Cu-Sn nanoparticles are de-

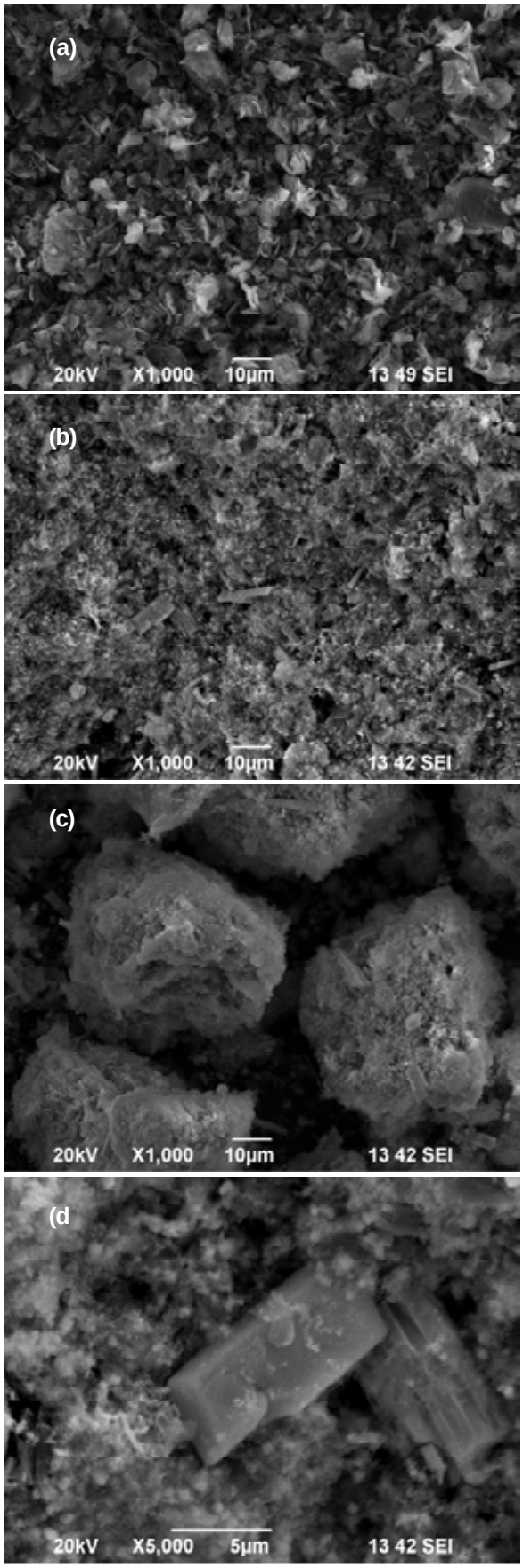


**Fig. 6.** SEM images at a different magnification: a - graphite, x1000, b, c - graphite/Cu-Sn nanoparticles, x1000, d-graphite/Cu-Sn nanoparticles, x5000.

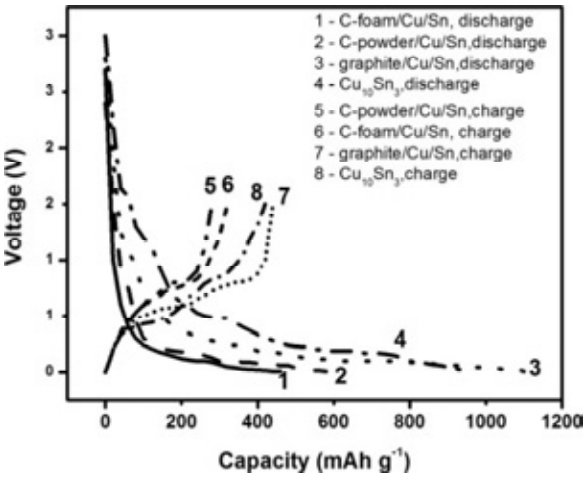


**Fig. 7.** Initial charge/discharge curves of $Cu_{10}Sn_3$ alloy and C/Cu-Sn composite electrodes.

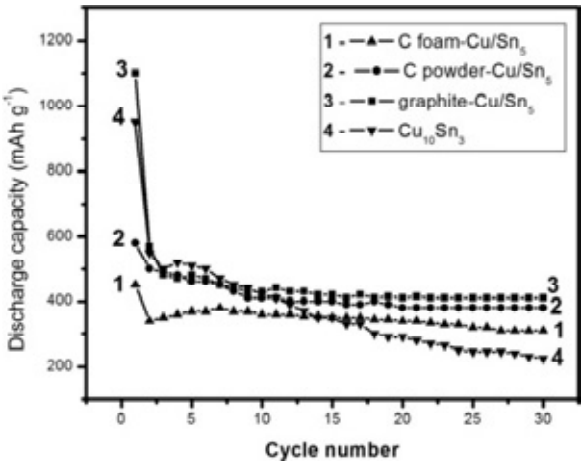


**Fig. 8.** Cycling performance of $Cu_{10}Sn_3$ alloy and C/Cu-Sn composite electrodes.

posited not only in the C-pores, but also on the C-grain surface. The mean particle size is 40 to 50 nm. The specific surface area of C-foam after the nanoparticle deposition is decreased from 17 to 15 $m^2.g^{-1}$. The phase composition of the Cu-Sn particles are characterized by the formation of Cu, Sn and $Cu_{10}Sn_3$ phases.

When C-powder is used as a support $Cu_6Sn_5$ phase is formed and a phase of $Cu_2O$ is also presented. The Cu-Sn nanoparticles 40 to 50 nm in size cover the C-grains like as a thin film. The specific surface area of C-powder after the nanoparticle deposition is decreased from 20 to 18 $m^2.g^{-1}$.

Cu-Sn nanoparticles obtained with graphite support are also aggregated and cover the graphite particles. The formed aggregated particles is about 50-60 μm in size. The specific surface area of graphite, whose grains are covered with Cu-Sn nanoparticles alloy is more lower – it is decreased from 4.8 to 3.8 $m^2\ g^{-1}$. In this case two main phases of $Cu_6Sn_5$ and $Cu_{10}Sn_3$ are established and also phase of $Cu_2O$ is presented.

In summary, it could be say that the different supports used influence not only on the particle size and their aggregation, respectively on the SSA, but also on the phase composition. Regardless of the support used the nanoparticle aggregation is strongly expressed due to their nanostate. The phase composition of the Cu-Sn nanoparticle alloy is depended differently on the support used. Two major Cu-Sn phases such as $Cu_{10}Sn_5$ or $Cu_6Sn_5$ are formed in the three cases when it is used different supports of C-foam, C-powder and graphite. Impure phases of Cu, $Cu_2O$, and Sn are also existed. As is known the phase composition of the active component (Cu-Sn alloy powder) in the C-based composites is of great importance for their electrochemical behavior.

The charge/discharge curves of the initial cycle for $Cu_{10}Sn_3$ alloy and C/Cu-Sn composites are shown in Fig. 7. The initial discharge curves exhibited two pronounced discharge plateaus at about 0.2 - 0.3 V and near 0.0 V for $Cu_{10}Sn_3$ alloy and composites. The discharge voltage above 0.3 V is attributed to lithium ions insert in $Cu_{10}Sn_3$ to form $Li_2CuSn$ , while the discharge voltage between 0.0 and 0.2 V corresponds to the formation of the fully lithiated Sn phase [25].

The charge curves also exhibited two plateaus at 0.5 V and 0.75 V for all materials. They correspond to the reversible formation of the $Li_2CuSn$ and $Cu_{10}Sn_3$ respectively.

The initial discharge/charge capacities of the composite powder electrodes are 1100/420mAh.$g^{-1}$ for the graphite/Cu-Sn composite; 580/280 mAh.$g^{-1}$ for the C-powder/ Cu-Sn composite; 450/330 mAh.$g^{-1}$ for the C-foam/Cu-Sn composite, and 950/450 mAh.$g^{-1}$ for the $Cu_{10}Sn_3$ alloy. All the electrodes with the exception of C-foam-Cu/Sn exhibit a large irreversible capacity at the initial charge-discharge cycle: 62% for the graphite/Cu-Sn composite; 52% for the C- powder /Cu-Sn composite and $Cu_{10}Sn_3$ alloy; 26% for the C-foam/Cu-Sn composite. The high irreversible capacity of the composite materials can be explained by the formation of the SEI film.

The volumetric capacity of the C/Cu-Sn composites and $Cu_{10}Sn_3$ alloy versus cycle number is plotted in Fig. 8. The different electrochemical behavior of the electrodes is due to their different phase composition and microstructure. The best cyclic stability on 30th cycle demonstrated the graphite/Cu-Sn composite (410 mAh.$g^{-1}$). In this case the depos-

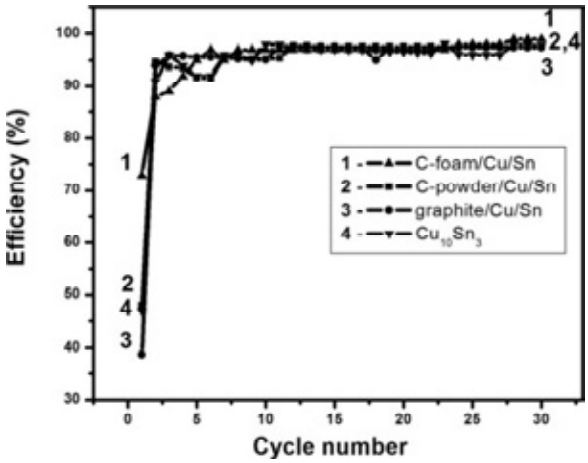


**Fig. 9.** Coulombic efficiencies *vs.* number of cycles for the C-Cu/Sn composite powders and $Cu_{10}Sn_3$ alloy.

ited tin particles undergo less mechanical stress during volume changes related to lithiation/ delitiation and did not lose contact with one another. The presence of various active sites in the composite such as $Cu_6Sn_5$, $Cu_{10}Sn_3$ facilitates the volumetric expansion and prevents the collapse of the electrode, because at a given voltage react only a part of the composite. In this case not lithiation phase acts as a buffer against the volumetric expansion on lithiation one. The reversible discharge capacity at 30th cycle for the other two composites of C-powder/Cu-Sn and C-foam/Cu-Sn are 380 mAh.g$^{-1}$ and 310 mAh.g$^{-1}$ respectively. The $Cu_{10}Sn_3$ alloy is characterized by the lowest reversible discharge capacity at 30th cycle (220 mAh.g$^{-1}$). The kinetics of the insertion and extraction of the Li from the anode material is gradually delayed with the number of cycles, because the deposited alloy becomes amorphous during the cycling as opposed to the C/Cu-Sn composites. In this case, only the copper coating is insufficient to soften the impact of the volume changes during the cycling.

The higher reversible discharge capacity of the composites is due to the formation of a stable microstructure of the Cu/Sn, involving the carbon material, which prevents the sputtering during the cycling process, and minimizes losses of the contact between the particles.

Fig. 9 shows the Coulombic efficiencies measured for electrodes produced using the three composites and $Cu_{10}Sn_3$ alloy. The initial Coulombic efficiencies of electrode produced using the composites, were as follows: 48% for the C-powder/ Cu-Sn composite, 73% for the C-foam/ Cu-Sn composite, 38% for the graphite-Cu/Sn composite, and 47% for the $Cu_{10}Sn_3$ alloy, respectively. During the subsequent cycles the electrodes exhibited high Coulombic efficiencies of 98-99% for all electrodes, indicating the high lithiation/delithiation reversibility in the powders.

## 4. CONCLUSION

The survey results suggest that regardless of the same technological conditions of a nanoparticle synthesis through a borohydride reduction by a template technique the electrochemical behavior of the obtained C/Cu-Sn composites is closely related to the type of the carbon matrix.

The type of the C-matrix influences on the phase composition of the active material and the morphology of the metal particles.

In the case of Cu-Sn alloy it is observed strongly aggregated particles having a size between 40-60 nm. The Cu-Sn alloy particles are in size 40-50 nm when both C-foam and C-powder are used as a matrix. In the case of C-foam the Cu-Sn nanoparticles are poorly aggregated, while in the case of C-powder a homogeneous nanostructured metal film covered the C-grains is formed. When using a matrix of graphite agglomerated graphite particles in size 50-60 μm coated with a thin Cu-Sn film were observed. Depending on the carbon matrix different composites are formed such as graphite/ $Cu_{10}Sn_3$, $Cu_6Sn_5$, $Cu_2O$; C- powder/ $Cu_6Sn_5$, $Cu_2O$; C- foam/ $Cu_{10}Sn_3$, Cu, Sn.

The reversible discharge capacity of the Cu-Sn alloy deposited on the various C-containing materials at 30th cycle increases from 220 mAh g$^{-1}$ to 310 mAh g$^{-1}$ for the C-foam/Cu-Sn composite; 380 mAh g$^{-1}$ for the C- powder/Cu-Sn composite and 410 mAh g$^{-1}$ for graphite/Cu-Sn composite. The C-foam/Cu-Sn composite is characterized by the highest efficiency at the first cycle of 73%. The effectiveness of the composites increased to 98-99% after the 5th cycle.

The graphite/ Cu-Sn composite is characterized by the highest irreversible discharge capacity of 62% and lower efficiency of the first cycle of 38% and also by the highest average discharge capacity. The high irreversible capacity can be explained by the presence of oxygenated impurities and formation of the SEI film. The best cyclibility is due to the presence of different active areas. Their attendance in the composite facilitates volume expansion and prevents disintegration of the electrode, since at a given voltage react only part of the composite. In this case unlithiated phase plays the role of a buffer against to the volumetric expansion of the lithiated one.

The selection of a suitable carbon matrix at the same conditions of the Cu-Sn alloy deposition could significantly improve its electrochemical behaviour. The three obtained composites are promising anode materials, an alternative to the graphite in lithium-ion batteries.

## ACKNOWLEDGEMENTS

This study was supported by the "Bulgarian Science Fund", Ministry of Education, Youth and Science of Bulgaria under the Project DVU 02/98 (No 862-UCTM).

## REFERENCES

[1] C.S. Wang, G.T. Wu, X.B. Zhang, Z.F. Qi and W.Z. Li // *J. Electrochem. Soc.* **145** (1998) 2751.
[2] F. Salrer-Disma, C. Lenair, B. Beaudoin, L. Aymard and J-M. Tarascon // *Solid State Ionics* **98** (1997) 145.
[3] D.A. Stevens and J.R. Dahn // *J. Electrochem. Soc.* **148 (**2001) 803.
[4] Y. Matsumura, S. Wang and J. Mondori // *J. Electrochem. Soc*. **142** (1995) 2914.
[5] P. Arora, R.E. White and M. Doyle // *J. Electrochem. Soc*. **145** (1998) 3647.
[6] T. Osaka, T. Momma, Y. Matsumoto and Y. Uchida // *J. Electrochem. Soc*. **144** (1997) 1709.
[7] Y. Idota, T. Kubota, A. Matsufuji, Y. Maekawa and T. Miyasaka // *Science* **276** (1997) 1395.
[8] J.O. Besenhard, J. Yang and M. Winter // *J. Power Sources* **68** (1997) 87.
[9] M.M. Thackeray, J.T. Vaughey, A.J. Kahaian, K.D. Kepler and R. Benedek // *Electrochem. Commun*. **1** (1999) 111.
[10] H. Mukaibo, T. Osaka, P. Reale, S. Panero, B. Scrosati and M. Wachtler // *J. Power Sources* **132** (2004) 225.
[11] K.D. Kepler, J.T. Vaughey and M.M. Thackeray // *Electrochem. Solid State Lett.* **2** (1999) 307.
[12] L.Y. Beaulieu, S.D. Beattie, T.D. Hatchard and J.R. Dahn // *J. Electrochem. Soc*. **150** (2003) 419.
[13] T. Takamura, K. Sumiya, J. Suzuki, C. Yamada and K. Sekine // *J. Power Sources* **81** (1999) 368.
[14] J.Y. Lee, R. Zhang and Z. Liu // *J. Power Sources* **90** (2000) 70.
[15] B. Veeraraghavan, A. Durairajan, B. Haran, B. Popov and R. Guidotti // *J. Electrochem. Soc.* **149** (2002) 675.
[16] M. Egashira, H. Takatsuji, S. Okada and J. Yamaki // *J. Power Sources* **107** (2002) 56.
[17] G.X. Wang, L. Sun, D.H. Bradhurst, S.X. Dou and H.K. Liu // *J. Alloys Comp*. **306** (2000) 249.
[18] G.X. Wang, Jung-Ho Ahn, M.J. Lindsay, L. Sun, D.H. Bradhurst, S.X. Dou and H.K. Liu // *J. Power Sources* **97** (2001) 211.
[19] Y.S. Jang, J.H. Kim, S.H. Choi, K.M. Yang and Y.C. Kang // *Int. J. Electrochem. Sci.* **7** (2012) 12531.
[20] S. Lui, Q. Li, Y. Chen and F. Zhang // *J. Alloys Compd.* **478** (2009) 694.
[21] J.K. Lee, D.H. Ryu, J.B. Ju, Y.G. Shul, B.W. Cho and D. Park // *J. Power Sources* **107** (2002) 90.
[22] K. Zaghib, G. Nadeau and K. Kinoshita // *J. Electrochem. Soc*. **147** (2000) 2110.
[23] M. Winter, P. Novak and A. Monnier // *J. Electrochem. Soc.* **145** (1998) 428.
[24] I. Markova-Deneva // *J. Univ. Chem. Technol. Met.* **45** (2010) 351.
[25] R. Fong, U. von Sacken and J. Dahn // *J. Electrochem. Soc.* **137** (1999) 2009.